Journal of Materials Chemistry B

Accepted Manuscript

This article can be cited before page numbers have been issued, to do this please use: A. Mebert, C. Aimé, G. S. Alvarez, Y. Shi, S. A. Flor, S. Lucangioli, M. F. Desimone and T. Coradin, *J. Mater. Chem. B*, 2016, DOI: 10.1039/C6TB00281A.

ROYAL SOCIETY OF CHEMISTRY

www.rsc.org/materialsB

View Article Online
DOI: 10.1039/C6TB00281A

Silica core-shell particles for the dual delivery of gentamicin and rifamycin antibiotics.

Andrea M. Mebert[1,2], Carole Aimé[3], Gisela S. Alvarez[1,2], Yupeng Shi[3],Sabrina A. Flor[4], Silvia E. Lucangioli[4], Martin F. Desimone[1,2*], Thibaud Coradin[3*]

[1]*Universidad de Buenos Aires, Facultad de Farmacia y Bioquimica, Junin 956 Piso 3. (1113) Ciudad Autónoma de Buenos Aires, Argentina.*

[2]*IQUIMEFA-CONICET*

[3]*Sorbonne Universités, UPMC Univ Paris 06, CNRS, Collège de France, UMR 7574, Laboratoire de Chimie de la Matière Condensée de Paris, 11 Place Marcelin Berthelot, F-75005 Paris, France.*

[4]*CONICET - Universidad de Buenos Aires, Facultad de Farmacia y Bioquímica, Departamento de Tecnología Farmacéutica. Ciudad Autónoma de Buenos Aires, Argentina.*

[*]Corresponding author email: desimone@ffyb.uba.ar

ABSTRACT

Increasing bacterial resistance calls for the simultaneous delivery of multiple antibiotics. One strategy is to design a unique pharmaceutical carrier that is able to incorporate several drugs with different physico-chemical properties. This is highly challenging as it may require the development of compartmentalization approaches. Here we have prepared core-shell silica particles allowing for the dual delivery of gentamicin and rifamycin. The effect

View Article Online
DOI: 10.1039/C6TB00281A

of silica particle surface functionalization on antibiotic sorption was first studied, enlightening the role of electrostatic and hydrophobic interactions. This in turn dictates the chemical conditions for shell deposition and further sorption of these antibiotics. In particular, the silica shell deposition was favored by the positively-charged layer of gentamicin coating on the core particle surface. Shell modification by thiol groups finally allowed for rifamycin sorption. The antibacterial activity of the core-shell particles against *Staphylococcus aureus* and *Pseudomonas aeruginosa* demonstrated the dual release and action of the two antibiotics.

View Article Online
DOI: 10.1039/C6TB00281A

1. INTRODUCTION

Drug carriers for local antibiotics delivery have gained attention in the last years due to the need to deliver effective antibiotic doses, and avoid the high toxicity associated with systemic administration [1]. Those delivery systems can be applied in situations such as periodontal disease [2], orthopedic trauma [3-5] or in skin wound healing [6]. However, due to the presence of multiple pathogens, and the increasing drug resistance, the co-delivery of different antibiotics or other compounds is a promising alternative for increasing treatment efficacy [7].

When the antimicrobial treatment is associated with the implantation of a biomaterial, the relevant drugs are ideally loaded within the biomaterial scaffold or at its surface[8]. However, for soft tissue repair where hydrogel-based dressings are used, the kinetics of drug release is usually too fast due to the large porosity of the scaffold compared to antibiotic dimensions[9]. Another strategy is to introduce strong chemical bonds between the material and the drug but this can become complex if multiple drug delivery is targeted.

As an alternative, the use of nanocomposite materials where the drugs are associated with nanoparticles embedded in the scaffold have attracted increasing attention[10, 11]. The intrinsic properties of these nanoparticles, as well as their interactions with the host hydrogel can be tuned so as to optimize the drug release profiles. Among possible antibiotic carriers, silica nanoparticles have been extensively studied. They can be prepared in a wide range of size, porosity and chemical composition. Whereas a full assessment of their biocompatibility is still to be achieved[12], numerous studies have demonstrated that silica nanoparticles with size ranging from 10 nm to 200 nm exhibit limited cytotoxicity[13-16].

View Article Online
DOI: 10.1039/C6TB00281A

Moreover, grafting sulfonate, amine and especiallythiol moieties further decreases their detrimental effect[17].

To address the issues related to co-delivery of antibiotics, two options can be envisioned. The first one would rely on the incorporation of different populations of particles, each loaded with a unique drug. Although each drug-carrier can be individually optimized, this approach requires the use of a high total concentration of silica particles. Alternatively, the incorporation of multiple drugs within a single type of particle can be envisioned. However, because the different drugs exhibit sometimes diverging physico-chemical properties (charge, hydrophobicity), a chemical compartmentalization is required for the design of the carrier particle. A rather simple option is to use core-shell nanoparticles, consisting of a core, or inner material surrounded by a shell, or outer layer[18]. Core-shell nanoparticles are widely used for bioimaging[19] and biosensing[20], as well as for other biomedical applications including theco-delivery of drugs[21, 22]. In particular, silica-based core-shell particles are commonly formed from a metal[23, 24], metal oxide[25, 26] or micellar core covered with a silica shell[27]. This outer layer gives the particle the same properties than silica particles, such as lower reactivity, enhanced stability in suspension and slower drug release [28]. Core-shell particles entirely formed by silica have also been reported exhibiting different characteristics such as bimodal pore structures [29] or selective functionalization of the inner and outer regions of the particles using hybrid sols[30].

Inspired by the latter approach, we report here a new type of silica core-shell particles having the capability to simultaneously deliver two common topical antibiotics, gentamicin and rifamycin. For this purpose, we have developed a strategy similar to layer-by-layer deposition routes where the positively-charged coating of the drugs on the core surface can act as the reactive interface for silica shell deposition. The role of electrostatic

View Article Online
DOI: 10.1039/C6TB00281A

and hydrophobic interactions between silanes and antibiotics on the successful synthesis of these core-shell particles is discussed, enlightening the foreseeable versatility of this approach.

2. MATERIALS AND METHODS

2.1 Materials

Tetraethyl orthosilicate (TEOS, 98 %), (3-aminopropyl)triethoxysilane (APTES, ≥98%) and (3-mercaptopropyl)trimethoxysilane (MPTMOS, ≥95%) were purchased from Sigma-Aldrich, as well as the antibiotics sodium rifamycin and gentamicin sulfate. Ammonium hydroxide (30%) was obtained from Carlo Erba Reagents. All other reagents were of analytical grade and commercially available.

2.2. Synthesis of silica particles

2.2.1. Silica particles (SiOH)

Bare silica particles were synthesized according to the Stöber method[31]. Briefly, 21 mL tetraethyl orthosilicate were added dropwiseto a stirred solution of 32 mL ultrapure water, 600 mL absolute ethanol, and 45 mL ammonium hydroxide. The solution was stirred overnight at room temperature. Particles were washed twice with absolute ethanol, once with deionized water and recovered by centrifugation, dried in vacuum and stored in a closed flask.

View Article Online
DOI: 10.1039/C6TB00281A

2.2.2. Amino modified silica particles ($SiNH_2$)

1mmol APTES per gram of SiOH was added to the reaction medium before washing. The solution was stirred overnight at room temperature and then washed and recovered as described before.

2.2.3. Thiol modified silica particles (SiSH)

5.51g unmodified SiOH particles were resuspended in a mixture of 548 mL absolute ethanol and 12 mL ammonium hydroxide, then 5.3 mL MPTMOS was added. It was stirred 40 minutes at room temperature and then the solvent was evaporated at 80ºC until 1/3 of the original volume was reached. Particles were washed twice with absolute ethanol, once with deionized water and recovered by centrifugation, dried in vacuum and stored in a closed flask.

2.2.4. Sulfonate modified silica particles ($SiSO_3$)

3.6g thiol modified NPs (SiSH) were resuspended in 180 mL hydrogen peroxide 35% and left 48 hours under stirring. Then the particles were washed three times with ethanol and dried in vacuum. The powered was resuspended and stirred in 150 mL sulfuric acid for two hours. Slowly the solution was diluted in deionized water in a cold bath. The particles were recovered and washed with ethanol and deionized water by centrifugation, vacuum dried and stored[32].

2.3. Particles loading

Antibiotic-loaded particles were prepared in deionized water by mixing the particles and the corresponding antibiotic, in a ratio of 375 mg particles: 20 mg antibiotic: 50 mL

View Article Online
DOI: 10.1039/C6TB00281A

deionized water. Suspensions were stirred overnight at room temperature and protected from light. The resulting particles were recovered by centrifugation and washed three times with deionized water. Sodium rifamycin and gentamicin sulfate were used as antibiotics.

2.4. Preparation of core-shell particles

The core was synthesized by the Stöber method, modified with thiol or sulfonate for the loading of rifamicyn or gentamicin respectively as described before. The silica shell layer synthesis was carried on with drug in the ethanol-water medium, in a ratio 500 mg particles : 27 mg antibiotic : 0.4 mL TEOS : 0.5 mL ammonium hydroxide : 1.5 ml deionized water : 50 mL ethanol. This shell was modified as described before to achieve core sulfonate-modified and shell thiol-modified particles ($SiSO_3$@SiSH) or core thiol-modified and shell sulfonate-modified particles (SiSH@$SiSO_3$). The second layer was loaded with the second antibiotic (i.e. that was not used in the first step) in the same drug : particles : deionized water ratio. The loaded core-shell particles were then washed and resuspended as described before.

2.5. Transmission Electron Microscopy (TEM)

The size and shape of the particles were investigated by TEM. Briefly a drop of sample in aqueous solution was deposited on 400-mesh carbon-coated copper grids. After one minute, the liquid was blotted with filter paper (Whatman no. 4). TEM was performed at room temperature using a JEOL 1011 electron microscope operating at 100 kV.

View Article Online
DOI: 10.1039/C6TB00281A

2.6. Zeta potential

The zeta potential of the particles was measured with Zeta Plus Brookhaven equipment. For this purpose a 5 $mg.mL^{-1}$suspension of particles was prepared in 10 mMKCl aqueous solution. In another experiment, 0.5 $mg.mL^{-1}$ particles were confronted to increasing concentrations of antibiotics. After each step of antibiotics addition, particles were recovered by centrifugation before zeta-potential measurement.

2.7. Microbiological assay (Diffusion Method)

The microbiological assay carried out using the disk diffusion method as described in the United States Pharmacopeia. Petri dishes with 2 to 5 mm thick Luria Bertani (LB) agar medium were inoculated and homogeneously scattered with 100 µL of 1 x 10^7 cfu ml^{-1} in PBS of the bacteria suspension sensitive to the antibiotic of interest. Sterile absorbent paper disks were impregnated with 10 µL of the particles suspension and placed on the surface of the agar. *Staphylococcus aureus* ATCC 29213 (sensitive to rifamycin and gentamicin) and *Pseudomonas aeruginosa* ATCC 27853 (sensitive to gentamicin) were used. The inhibition zone was measured after incubation at 37ºC for 24 hours, and evaluated using the corresponding calibration curve of antibiotics selected according to the known sensitivity of the microorganisms to the antibiotic of interest (i.e.: 20-60 $\mu g.mL^{-1}$ for gentamicin, and 0.3-1.2 $\mu g.mL^{-1}$ for rifamycin). In all cases results are expressed as mean $\pm$ SD from triplicate experiments.

View Article Online
DOI: 10.1039/C6TB00281A

2.8. Quantification of gentamicin and ryfamicin.

The kinetics of the dual drug release behaviour of core-shell particles was determined by Mass Spectrometry. Nanoparticles were suspended at a 30 $mg.mL^{-1}$ concentration in deionized water at 37°C. At regular interval of time, they were recovered by centrifugation and the amount of drug released was measured by MS. For this purpose, quantitative and qualitative mass analysis was carried out on a TSQ Quantum Access™ Max (Thermo Fisher Scientific, San Jose, CA, USA) triple stage quadrupole mass spectrometer with an electrospray ionization (ESI) source and a Rheodyne™ 7750E-185 divert/inject valve. Sample injection was performed via the Rheodyne injection valve with a 10 µl loop. Linearity of the detector response to sample concentration was assessed by measuring five calibration points ranging from 5 to 600 $ng.mL^{-1}$ for gentamicin and rifamycine. Each calibration point was injected five times. Regression coefficients were obtained by plotting the average peak area versus concentration, using the least squares method (**ESI-1**). Three ions were selected for the quantification of gentamicin (m/z 464, 322 and 160) and rifamycin (720, 660 and 574).

2.9. Statistical analysis

In all cases data are means $\pm$ SD of triplicate experiments. The differences were analyzed using two-way ANOVA, followed by the Tukey post-test; $p < 0.05$ was considered significant.

View Article Online
DOI: 10.1039/C6TB00281A

3. RESULTS AND DISCUSSION

3.1 Characterization of surface-modified silica particles

Monodisperse spherical silica particles were obtained by the Stöber method[31, 32]. The mean diameter for each type of particles was 277 ± 12 nm (SiOH), 273 ± 5 nm ($SiNH_2$), 269 ± 7 nm (SiSH) and 277 ± 2 nm ($SiSO_3$) as determined by TEM (**Fig. 1a-b**), indicating that the particle mean diameter was not significantly affected by the surface modification (**ESI-2**). The surface modification was also analyzed by measuring the zeta potential (ζ) of the particles at different pHs (**Fig. 1c**). Starting from pH 2, the bare silica particles (SiOH) are slightly positively charged and undergo a rapid surface charge reversal between pH 3 and 4 before reaching a constant value of ca. – 65 mV. For thiol-bearing particles (SiSH), the ζ value is almost zero in acidic media and reaches ca. -30 mV at pH 8. After sulfonation, the ζ value is negative over the whole range of pH, with a slight decay between pH 3 and 5. Finally, the ζ value of amino-modified particles ($SiNH_2$) follows a similar trend except that values go from highly positive (+ 65 mV) to zero.

The measured evolution for bare silica nanoparticles is in good agreement with the literature, indicating that silanols can exist in three different forms on silica surface: $SiOH_2^+$, SiOH and SiO^-. The positively-charged species are present in significant amount up to pH *ca*. 3. This is in agreement with the point of zero charge of 3 for ca. 270 nm silica particles as reported elsewhere[33]. Then it was suggested that further deprotonation involves two populations of silanol groups, 20 % being acidic ($pKaSiOH/SiO^-$ = 4.5) and 80 % basic ($pKaSiOH/SiO^-$ = 8.5). In the case of thiol groups, with a pKa (SH/S^-) of *ca*. 10.5, the organic function should not contribute to the surface charge of the particle in the investigated pH range. Therefore the observed ζ evolution can be attributed to the decrease

View Article Online
DOI: 10.1039/C6TB00281A

of available silanol groups on the particle surface after grafting, leading to a lower density of $SiOH_2^+$ in acidic media and SiO^- in basic solution, therefore narrowing the range of ζ variation. After sulfonation, the strongly acidic SO_3^- groups (pKa SO_3H/SO_3^-<1) should contribute to a constant negative charge that can be evidenced at low pH.However, in basic medium, the absolute value of ζ for sulfonated particles is smaller than for bare silica particles. This indicates that, from a surface charge point of view, the decrease in the number of free silanol groups on the silica surface that results from the grafting reaction is not compensated by the presence of sulfonate groups on the organic chain of the silane. Accordingly, since pKa of primary amines is *ca*. 10.5, their protonation degree should be constant over the 2-8 pH range of this study and should therefore contribute in a constant manner to the surface charge of $SiNH_2$ particles. Comparison of the ζ evolution of $SiNH_2$ and SiOH shows that this is indeed the case except in the 3-4 pH range. This probably reflects the existence of direct acid-base reactions between surface silanolate and ammonium groups from APTES, as reported in the literature [34].

3.2 Characterization of antibiotic-coated silica particles

Silica particles were loaded with two oppositely charged antibiotics, gentamicin being positively charged, while rifamycin is negatively charged. TEM analysis revealed that particle mean diameter was not significantly affected by the antibiotic adsorption (**ESI-3**). Based on preliminary experiments, particles loading were performed in a large excess of antibiotics (20 mg antibiotics for 375mg particles in water). After washing, the gentamicin and rifamycin loadings were evaluated on *P. aeruginosa* and *S. aureus*, respectively. Antibiograms were carried out using the disk diffusion method, and inhibition zones

View Article Online
DOI: 10.1039/C6TB00281A

measured after incubation for 24 h at 37ºC. After this period, impregnated paper discs were transferred to a new agar media seeded with bacteria and incubated for an additional 24 h period. However, no antibacterial activity could be observed after this delay, suggesting that a major fraction of the antibiotics was released over the first 24 h. Unloaded particles showed no antibacterial activity in all cases indicating that the measured bactericidal effects originated from the drugs only.

In the case of gentamicin, the largest antibiotic amount was found for the most negatively-charged particles SiOH and $SiSO_3^-$ compared to thiol- (SiSH) and amino- ($SiNH_2$) modified silica particles (**Fig. 2**). This suggests that attractive electrostatic interactions are the main driving force for the sorption process. Indeed, the amounts of gentamicin in SiOH and $SiSO_3^-$ are 1509 $\mu g.g^{-1}$ and 1793 $\mu g.g^{-1}$, respectively, which are 6 and 7 times higher than the amount found in SiSH (**Table 1**).

On the other hand, in the case of the negatively-charged rifamycin, the situation is more complex. Despite their positively-charged surface, $SiNH_2$ particles do not adsorb significantly more antibiotic than bare particles. Moreover, the highest rifamycin loading was obtained for slightly negatively-charged SiSH particles with 19.2 $\mu g.g^{-1}$ (**Table 1**). This can be explained considering that rifamycin is classified as an hydrophobic molecule, with an octanol-water partition coefficient of 2.77 [35], while thiol groups have the capability to confer non polar-properties to modified surfaces [36, 37]. Therefore it is very likely that hydrophobic interactions are involved in the rifamycin sorption on SiSH. Sulfonated particles were not evaluated as their negative surface charge was expected to repel anionic rifamycin molecules.

To clarify the sorption process, the evolution of zeta potential with antibiotic concentration was studied for the antibiotic-loaded particles that exhibited even a low antimicrobial

View Article Online
DOI: 10.1039/C6TB00281A

activity, namely $SiSO_3$, SiOH, and SiSH for gentamicin, and $SiNH_2$, and SiSH for rifamycin. In the case of gentamicin adsorption, a gradual increase in the ζ value with antibiotic concentration was observed for SiOH, $SiSO_3^-$ and SiSH up to slightly positive values (+5/+15 mV, **Fig. 3**). The difference in ζ value between uncoated and saturated surfaces for each type of particles nicely correlates with the drug loading as determined by the disk method. Altogether, this supports the previous hypothesis that the sorption process is driven by attractive electrostatic interactions and that saturation occurs after neutralization of the negative charge of the particle surface by positively-charged gentamicin. Nevertheless, it must be noticed that the final ζ value is slightly positive. This suggests that a fraction of the antibiotic is adsorbed*via* other interactions either with the silica surface or with already-deposited molecules. In particular, the presence of three hydroxyl groups on the gentamicin backbone should favor hydrogen bond formation.

In the case of rifamycin, the relationship between zeta-potential and drug adsorption is not straightforward. Addition of a small amount of antibiotic leads to a decrease of ζ for both SiSH and $SiNH_2$. This event is more pronounced for the former than for the latter, suggesting that it corresponds to the adsorption of the negatively-charged antibiotics. Increasing further the antibiotic concentration does not significantly modify the ζ value, but a slight continuous increase is obtained for SiSH. Since the rifamycin loading capacity of these two systems is about hundred times lower than for gentamicin (see **Table 1**), it can be expected that surface saturation is reached at such low concentrations. Moreover, near neutral pH, gentamicin bears five positive charges per molecule, whereas rifamycin has only one negatively-charged group so that the former should have more influence on the overall particle surface charge than the latter at a similar surface concentration (**Fig. 4**). As

View Article Online
DOI: 10.1039/C6TB00281A

a matter of fact, the two drugs also differ from the point of view of the accessibility of the ionized groups. In gentamicin structure, the ammonium functions point out of the glycosidic rings, whereas the OH group of rifamycin belongs to a naphtalene ring inducing a sterical barrier and conferring a strong hydrophobic character to the molecule. This can explain its low sorption on $SiNH_2$ particles despite their high positive charge. It also strengthens our hypothesis about the key role of hydrophobic interactions on rifamycin sorption.

3.3. Core-shell nanoparticles and their dual antibiotic drug release properties

In a step forward, particles capable of releasing two antibiotics were designed. Our strategy involves the synthesis and functionalization of a Stöber silica core and its loading with the first antibiotic (drug A), followed by deposition of the shell that is further functionalized and loaded with the second antibiotic (drug B) (**Fig. 5**). The evolution of the particle size, as determined by DLS, and of their surface charge, as obtained by ζ measurements, are provided in **Table 2** at each step of the preparation process.

A first configuration was studied using the sulfonated core loaded with gentamicin, as it exhibited the higher drug loading, further coated with a silica shell and functionalized with thiol groups followed by rifamycin sorption ($SiSO_3$-G@SiSH-R). ζ data show that the adsorption of gentamycin on $SiSO_3$ leads to a decrease in negative charge of the particles, as expected for the deposition of the cationic antibiotic. DLS also indicate a slight increase in the particle diameter. Note that these data were obtained after rinsing the particles so that, compared to the values obtained in the presence of an excess of antibiotics and representative of the synthesis process (**Fig. 3**), partial gentamycin desorption has occurred

View Article Online
DOI: 10.1039/C6TB00281A

leading to a negative value of ζ. Subsequently, reaction of $SiSO_3$-G with TEOS leads to an increase of the absolute value of ζ, reaching ca. -60 mV and therefore close to the value of bare Si-OH particles, strongly supporting the formation of a silica shell. In parallel, DLS data also suggest an increase in particle diameter but the relatively high value of the standard deviation for $SiSO_3$-G (40 nm) does not allow the calculation of the shell thickness. After outer grafting with MPTMOS, the ζ decreases in absolute value, similarly to our previous observation of MPTMOS reaction on core silica particles. The successful formation and functionalization of the shell was also supported by analyzing the pH dependence of the ζ value of the particles after synthesis (**Fig. 6**). The evolution of the zeta potential in the pH range 2 to 8 closely follows that of the thiolated core particles, indicating that the resulting surface chemistry are similar. Finally, further contact with rifamycin decreases again the absolute value of ζ. In parallel, DLS data suggest an important aggregation of the particles.

The mirror situation using the thiolated core loaded with rifamycin coated with a silica shell and functionalized with sulfonated groups, followed by gentamycin sorption (SiSH-R@$SiSO_3$-G) was studied. As seen in **Table 2**, after contact of TEOS with the rifamycin-coated thiolated core particles, only a slight variation of ζ is measured for the expected (SiSH-R@SiOH) system and this value is not significantly modified after MPTMOS grafting and sulfonation (SiSH-R@$SiSO_3$). In parallel all particle sizes obtained from DLS were within the standard deviation range, except for the final gentamycin deposition. A more detailed study of the pH-dependence of the ζ for SiSH-R@$SiSO_3$ systems show that it follows that of sulfonated cores but with a significantly more negative value in acidic conditions (**Fig. 6**). This suggests that the oxidation reaction required for

View Article Online
DOI: 10.1039/C6TB00281A

sulfonation of thiol groups of the shell also impact on the thiol groups present on the core particle. In addition, the experimental conditions for the sulfonation of the shell are particularly harsh when considering the shell formation of preloaded cores, involving a multistep process with hydrogen peroxide, sulfuric acid and successive washings. This suggests that such a combination is not suitable to obtain bi-functional core-shell particles so that only gentamicin loading of the core will be considered for the rest of the manuscript. The structure of the particles obtained with and without antibiotics was then analyzed by TEM. As can be seen in **Figure 7**, for antibiotic-free core particles, no significant modification of the surface of the final colloids was observed, even after the sorption of the second drug. In contrast, when gentamicin was initially deposited on the core particle, an additional thin layer was observed on the particle surface. This layer could still be observed after further shell surface sorption of rifamycin.

The deposition of a silica shell was confirmed by SEM imaging (**Fig. 8 and ESI-4**). The surface of the silica shell grown on the surface of gentamicin-coated $SiSO_3$ particles shows a granular aspect that is also strikingly observed after rifamycin sorption on these core-shell systems.

At this point, it is important to consider the shell process formation. The possibility to form SiO_2 shells on silica particles in the Stöber conditions has been widely described[38]. Although electrostatic interactions are unfavorable to silica deposition on bare silica particles, it may proceed thanks to the promotion of the condensation reaction of silanols and silonates in basic conditions. Surface modification by cationic coating introduces favorable electrostatic interactions promoting silica deposition[39]. On the opposite, introduction of anionic groups on the particle surface should limit shell formation. The effect of grafting hydrophobic moieties should also make the coating process of hydrophilic

View Article Online
DOI: 10.1039/C6TB00281A

silica less favorable than for bare particles. Coming back to our samples, the efficiency of the shell layer deposition of silica particles should vary as SiOH>SiSH> $SiSO_3$. Noticeably, TEM images could not provide any evidence that such reaction occurred in these conditions. However, this situation was changed after gentamicin sorption as the surface turned positive, favoring the formation of an observable silica shell. On this basis, only the $SiSO_3$@SiSH configuration was further studied.

Antimicrobial activity against the two bacterial strains (gentamicin-sensitive *P. aeruginosa*and gentamicin-rifamycin-sensitive *S. aureus*) was achieved when the two drugs were present within the core-shell particles. The diameters of the corresponding inhibition zones were taken as 100% to compare the efficiency of these dual systems with particles containing a single antibiotic (**Fig. 9**). For both bacteria, drug-free core-shell particles showed no significant antibacterial activity. For *P. aeruginosa*, the gentamicin-free particles were ineffective whereas the gentamicin-loaded particles showed an antibacterial activity similar to the particles with both antibiotics. This is in good agreement with the fact that rifamycin is poorly effective towards gram-negative bacteria. It is important to point out that gentamicin-coated core particles and core-shell systems have a similar antibacterial efficiency, indicating that no important leaching of gentamicin occurred from the particle core during rifamycin sorption on the shell. For *S. aureus*, the core-shell particles containing both drugs presented an antimicrobial activity 1.5 times higher than that of the two systems containing only one antibiotic. These results indicate that these core-shell particles can efficiently deliver both antibiotics.

To clarify this point, mass spectrometry analysis of a particle suspension supernatant allowed to identify the presence of gentamicin and rifamycin[40, 41] (**ESI-5**) and further confirmed the release of both antibiotics from the core-shell particles. The kinetics

View Article Online
DOI: 10.1039/C6TB00281A

profiles revealed that 43% of the rifamycin is released during the first 30 minutes while the release of the 50% of the gentamicin requires four times longer incubation times. Moreover, rifamycin is completely released from the particles within 3 hours while only 71% of the gentamicin is released over the same period (**Fig. 10**). This is in agreement with the proposed mechanism where the outer rifamycin coating is rapidly desorbed whereas gentamicin release requires the progressive diffusion through the silica shell or dissolution of the silica shell.

Our procedure has some similarities with layer-by-layer routes, where the core-shell structure is built up from alternation of coatings with opposite charges. Whereas a close strategy was previously described to build up bi-functional core-shell mesoporous particles using hybrid sols,[30] we have here taken advantage of the antibiotic layer itself as a charged interface for shell deposition, limiting its leaching during silica formation and further chemical modification. This strategy should therefore be applicable to any positively-charged drug as core component, whereas the shell coating may be of various natures. Importantly, although the mirror situation, *i.e.* direct shell coating from TEOS on a negatively-charged core, does not appear possible as such, the use of hybrid sols containing cationic silanes, such as TEOS/APTES mixtures, should allow for further silica deposition[42]. Accordingly, the use of hydrophobic sols can favor shell formation on the surface of core particles coated with lipophilic drugs[43].

This strategy can also be extended to mesoporous particles that may offer the possibility for the loading of up to four drugs (inside core, outside core, inside shell, outside shell) whose sequential release may be additionally tuned by gate-keeping approaches[44-46]. Such a strategy may be of particular interest in so-called combination therapy, that has become a key strategy in cancer treatment[47].

View Article Online
DOI: 10.1039/C6TB00281A

CONCLUSIONS

The co-encapsulation of drugs with different, and sometimes divergent, physico-chemical properties within a single carrier requires the development of compartmentalization strategies. The core-shell approach appears particularly suitable for this purpose but faces possible interference in the presence of drugs associated with the core particle with further deposition of the shell. On the contrary, we show here that it is possible to benefit from the presence of a positively-charged antibiotic coating to promote further silica deposition. This approach also has the advantage to avoid premature leaching of the core drug during shell formation. As a step further, it is now important to extend this layer-by-layer strategy to anionic and hydrophobic drugs. In addition, further control of shell structure should allow for a temporally differentiated control of the release kinetics of the two molecules.

ACKNOWLEDGEMENTS

A. M. Mebert is grateful for her doctoral fellowship granted by the National Research Council (CONICET). Y. Shi is funded by the China Scholarship Council. The authors would like to acknowledge the support of grants from the Universidad de Buenos Aires UBACYT 20020110100081, from CONICET PIP 11220120100657CO and from Agencia Nacional de Investigaciones Cientificas y Técnicas PICT 2012-1441 (to M. F. D). M.F.D. and T.C. thank the Argentina- France MINCYT-ECOS-Sud (project A12S01) and CONICET- CNRS programs for financial support of their collaboration. The authors would like to thank J. Nesterzak for his technical assistance.

View Article Online
DOI: 10.1039/C6TB00281A

Electronic supplementary information (ESI) available: Additional TEM and SEM images of nanoparticles and MS data of antibiotics. See DOI: 10.1039/

REFERENCES

1. G. Tiwari, R. Tiwari, B. Sriwastawa, L. Bhati, S. Pandey, P. Pandey and S. K. Bannerjee, *Int J Pharm Inv*, 2012, **2**, 2-11.
2. N. J. Medlicott, M. J. Rathbone, I. G. Tucker and D. W. Holborow, *Adv Drug Deliver Rev*, 1994, **13**, 181-203.
3. I. Hornyxak, E. Madacsi, P. Kalugyer, G. Vacz, D. B. Horvathy, M. Szendroi, W. Han and Z. Lacza, *BioMed Res Int*, 2014, **2014**, 8.
4. S. J. McConoughey, R. P. Howlin, J. Wiseman, P. Stoodley and J. H. Calhoun, *J Biomed Mater Res B: Appl Biomater*, 2015, **103**, 870-877.
5. A. R. Short, D. Koralla, A. Deshmukh, B. Wissel, B. Stocker, M. Calhoun, D. Dean and J. O. Winter, *J Mater Chem B*, 2015, **3**, 7818-7830.
6. A. Saito, H. Miyazaki, T. Fujie, S. Ohtsubo, M. Kinoshita, D. Saitoh and S. Takeoka, *Acta Biomater*, 2012, **8**, 2932-2940.
7. T. Bollenbach, *Curr Op Microbiol*, 2015, **27**, 1-9.
8. A. Santos, M. Sinn Aw, M. Bariana, T. Kumeria, Y. Wang and D. Losic, *J Mater Chem B*, 2014, **2**, 6157-6182.
9. M. Zilberman, D. Egozi, M. Shemesh, A. Keren, E. Mazor, M. Baranes-Zeevi, N. Goldstein, I. Berdicevsky, A. Gilhar and Y. Ullmann, *Acta Biomater*, 2015.
10. G. S. Alvarez, C. Helary, A. M. Mebert, X. Wang, T. Coradin and M. F. Desimone, *J Mater Chem B*, 2014, **2**, 4660-4670.
11. B. Song, C. Wu and J. Chang, *Acta Biomater*, 2012, **8**, 1901-1907.
12. Y. Wang, A. Santos, A. Evdokiou and D. Losic, *J Mater Chem B*, 2015, **3**, 7153-7172.
13. H. Zhang, D. R. Dunphy, X. Jiang, H. Meng, B. Sun, D. Tarn, M. Xue, X. Wang, S. Lin, Z. Ji, R. Li, F. L. Garcia, J. Yang, M. L. Kirk, T. Xia, J. I. Zink, A. Nel and C. J. Brinker, *J Am Chem Soc*, 2012, **134**, 15790-15804.
14. D. Lison, L. C. J. Thomassen, V. Rabolli, L. Gonzalez, D. Napierska, J. W. Seo, M. Kirsch-Volders, P. Hoet, C. E. A. Kirschhock and J. A. Martens, *Toxicol Sci*, 2008, **104**, 155-162.
15. D. Napierska, L. C. J. Thomassen, V. Rabolli, D. Lison, L. Gonzalez, M. Kirsch-Volders, J. A. Martens and P. H. Hoet, *Small*, 2009, **5**, 846-853.
16. S. Quignard, G. Mosser, M. Boissière and T. Coradin, *Biomaterials*, 2012, **33**, 4431-4442.
17. C. G. Gonzalez, G. S. Álvarez, D. E. Camporotondi, M. L. Foglia, C. Aimé, L. E. Diaz, T. Coradin and M. F. Desimone, *Silicon*, 2014, DOI 10.1007/s12633-12014-19203-12635.
18. R. Ghosh Chaudhuri and S. Paria, *Chem Rev*, 2012, **112**, 2373-2433.
19. T.-J. Yoon, K. N. Yu, E. Kim, J. S. Kim, B. G. Kim, S.-H. Yun, B.-H. Sohn, M.-H. Cho, J.-K. Lee and S. B. Park, *Small*, 2006, **2**, 209-215.

View Article Online
DOI: 10.1039/C6TB00281A

20. I. Al-Ogaidi, H. Gou, A. K. A. Al-kazaz, Z. P. Aguilar, A. K. Melconian, P. Zheng and N. Wu, *Anal Chim Acta*, 2014, **811**, 76-80.
21. Y. Wang, S. Gao, W.-H. Ye, H. S. Yoon and Y.-Y. Yang, *Nat Mater*, 2006, **5**, 791-796.
22. G.-F. Luo, W.-H. Chen, Y. Liu, Q. Lei, R.-X. Zhuo and X.-Z. Zhang, *Sci. Rep.*, 2014, **4**.
23. H. U. Lee, C. Park and S. W. Kim, *Proc Biochem*, 2012, **47**, 1282-1286.
24. S. C. Larsen, S. E. Lehman, A. S. Morris, P. S. Mueller, A. Salem and V. Grassian, *Environmental Science: Nano*, 2015.
25. A. A. Ansari and M. Alam, *J Lumin*, 2015, **157**, 257-263.
26. F. Jiang, Y. Fu, Y. Zhu, Z. Tang and P. Sheng, *J Alloys Comp*, 2012, **543**, 43-48.
27. J. Liu, C. Detrembleur, S. Mornet, C. Jérôme and E. Duguet, *J Mater Chem B*, 2015, **3**, 6117-6147.
28. Q. Huo, J. Liu, L.-Q. Wang, Y. Jiang, T. N. Lambert and E. Fang, *J Am Chem Soc*, 2006, **128**, 6447-6453.
29. H. Ishii, T. Ikuno, A. Shimojima and T. Okubo, *J Colloid Int Sci*, 2015, **448**, 57-64.
30. V. Cauda, A. Schlossbauer, J. Kecht, A. Zürner and T. Bein, *J Am Chem Soc*, 2009, **131**, 11361-11370.
31. L. C. J. Thomassen, A. Aerts, V. Rabolli, D. Lison, L. Gonzalez, M. Kirsch-Volders, D. Napierska, P. H. Hoet, C. E. A. Kirschhock and J. A. Martens, *Langmuir*, 2010, **26**, 328-335.
32. C. Aimé, G. Mosser, G. Pembouong, L. Bouteiller and T. Coradin, *Nanoscale*, 2012, **4**, 7127-7134.
33. S. V. Patwardhan, F. S. Emami, R. J. Berry, S. E. Jones, R. R. Naik, O. Deschaume, H. Heinz and C. C. Perry, *J Am Chem Soc*, 2012, **134**, 6244-6256.
34. R. G. Acres, A. V. Ellis, J. Alvino, C. E. Lenahan, D. A. Khodakov, G. F. Metha and G. G. Andersson, *J Phys Chem C*, 2012, **116**, 6289-6297.
35. W. H. Cover and S. C. Rittenberg, *J Bacteriol*, 1984, **157**, 391-397.
36. H. Niu, S. Wang, T. Zeng, Y. Wang, X. Zhang, Z. Meng and Y. Cai, *J Mater Chem*, 2012, **22**, 15644-15653.
37. M. H. Marchena, M. Granada, A. V. Bordoni, M. Joselevich, H. Troiani, F. J. Williams and A. Wolosiuk, *J Solid State Chem*, 2012, **187**, 97-102.
38. A. van Blaaderen and A. Vrij, *Langmuir*, 1992, **8**, 2921-2931.
39. T. Coradin, E. Mercey, L. Lisnard and J. Livage, *Chem Comm*, 2001, 2496-2497.
40. N. Isoherranen and S. Soback, *Analyst*, 2000, **125**, 1573-1576.
41. B. Prasad and S. Singh, *Journal of Pharmaceutical and Biomedical Analysis*, 2010, **52**, 377-383.
42. S. Sakai, T. Ono, H. Ijima and K. Kawakami, *Biomaterials*, 2001, **22**, 2827-2834.
43. S. Li, X. Jiao and H. Yang, *Langmuir*, 2013, **29**, 1228-1237.
44. I. I. Slowing, J. L. Vivero-Escoto, C. W. Wu and V. S. Y. Lin, *Adv Drug Deliver Rev*, 2008, **60**, 1278-1288.
45. L. Palanikumar, E. S. Choi, J. Y. Cheon, S. H. Joo and J. H. Ryu, *Adv Functional Mater*, 2015, **25**, 957-965.
46. T. Chen, W. Wu, H. Xiao, Y. Chen, M. Chen and J. Li, *ACS Macro Lett*, 2016, **5**, 55-58.
47. S. Gadde, *MedChemComm*, 2015, **6**, 1916-1929.

View Article Online
DOI: 10.1039/C6TB00281A

View Article Online
DOI: 10.1039/C6TB00281A

Legends to figures

Figure 1: (a,b) TEM photo of unmodified SiOH particles. (c) Zeta-potential of sulfonate-modified ($SiSO_3$), unmodified (SiOH), amino-modified ($SiNH_2$) and thiol-modified (SiSH) silica particles at different pHs (10 mMKCl).

Figure 2: Disk diffusion method evaluation of the antibacterial activity. Activities expressed as International Units (IU) of drug per gram of particles: (A) gentamicin and (B) rifamycin. Results are expressed as mean +/- SD from at least triplicate experiments. * indicates statistical significant difference. ($p< 0.0001$).

Figure 3: Zeta-potential of silica particles as a function of antibiotic concentration. (A) Gentamicin-loaded sulfonate ($SiSO_3$-G), unmodified (SiOH-G), and thiol (SiSH-G) modified particles. (B) Rifamycin loaded amino ($SiNH_2$-R) and thiol (SiSH-R) modified particles.

Figure 4: Chemical structures of (A) gentamicin and (B) rifamycin.

Figure 5: Scheme of the synthesis of double drug-loaded core-shell particles based on a two steps Stöber process.

Figure 6: Zeta-potential of silica particles and core-shell particles as a function of pH: SiSH-R@$SiSO_3$ as compared with $SiSO_3$, and $SiSO_3$-G@SH as compared with SiSH.

View Article Online
DOI: 10.1039/C6TB00281A

Figure 7: TEM images of: (A) SiOH@SiSH, (B) SiSH@SiSH and (C) $SiSO_3$@SiSHcore-shell particles, with or without gentamicin (G)-loaded core and with or without rifamycin (R)-loaded shell (scale bar 50 nm).

Figure 8: SEM images of (A) $SiSO_3$@SiSH and (B) $SiSO_3$-G@SiSH-R particles (scale bar 50 nm).

Figure 9: Disk diffusion method evaluation of the antibacterial activity of core-shell particles: (A) plates obtained with (a) rifamycin calibration curve (0.3 – 0.6 – 1.2 $\mu g.ml^{-1}$), (b) $SiSO_3$@SiSH-R, (c) $SiSO_3$-G@SiSH-R, (d) $SiSO_3$-G@SiSH and (e) $SiSO_3$@SiSH on (i) *P. aeruginosa* (ii) *S. aureus*. (B) Corresponding diameter size relative to $SiSO_3$-G@SiSH-R (100%) for (i) *P. aeruginosa*and (ii) *S. aureus*. * and ** indicates statistical significant difference. ($p < 0.0001$).

Figure 10: Dual release profiles of rifamicyn and gentamicin from the core-shell particles measured by mass spectrometry.

View Article Online
DOI: 10.1039/C6TB00281A

Table 1. IU drug per gram and the corresponding µg per gram of particles (A) gentamicin and (B) rifamycin loaded particles. Results are expressed as mean +/- SD from at least triplicate experiments.

A)

Gentamicine	IU Drug / g NPs	µg Drug / g NPs
$SiSO_3^-$	1058 ± 256	1793 ± 467
SiOH	890 ± 11	1509 ± 20
SiSH	160 ± 240	271 ± 407
$SiNH_2$	0 ± 0	0 ± 0

B)

Rifamycin	IU Drug / g NPs	µg Drug / g NPs
SiSH	17.2 ± 3.2	19.2 ± 3.5
$SiNH_2$	0.6 ± 0.3	0.7 ± 0.4
SiOH	0.0 ± 0.0	0.0 ± 0.0

View Article Online
DOI: 10.1039/C6TB00281A

Table 2. Evolution of zeta potential (ζ) in 10 mMKCl and hydrodynamic diameter (d_H) as obtained from DLS in deionized water at each step of the bifunctional core-shell particles synthesis (G: gentamycin; R: rifamycin). Results are expressed as mean +/- SD from at least triplicate experiments.

sample	ζ (mV)	d_H (nm)	sample	ζ (mV)	d_H (nm)
$SiSO_3$	-50 ± 3	257 ±16	SiSH	- 38 ± 2	258 ± 7
$SiSO_3$-G	- 18 ± 1	325 ± 42	SiSH-R	- 32 ± 2	253 ± 17
$SiSO_3$-G@SiOH	- 59 ± 2	358± 17	SiSH-R@SiOH	- 55 ± 2	267 ± 5
$SiSO_3$-G@SiSH	- 32 ± 1	377±13	SiSH-R@$SiSO_3$	- 46 ± 2	275 ± 13
$SiSO_3$-G@SiSH-R	-13 ± 2	1240 ± 157	SiSH-R@$SiSO_3$-G	- 6 ± 1	988 ± 130

View Article Online
DOI: 10.1039/C6TB00281A

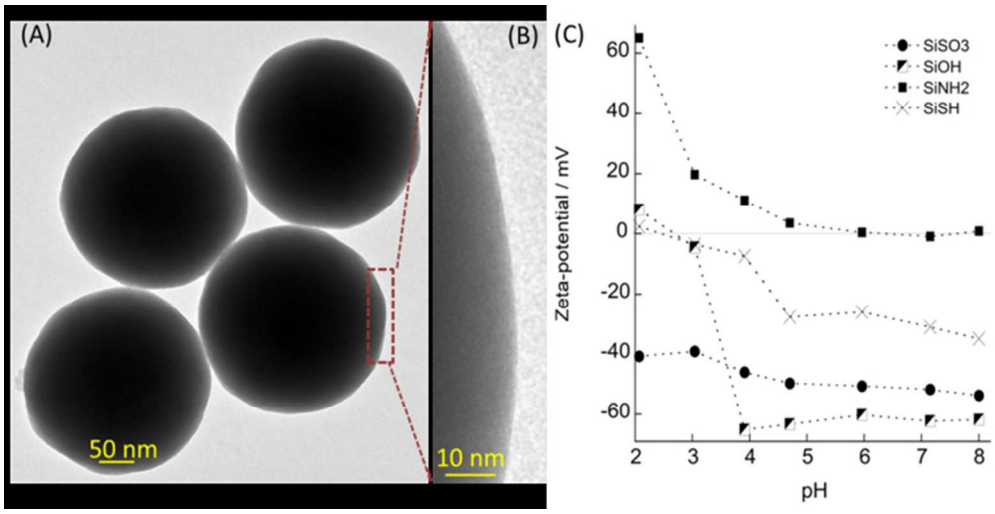

Figure 1: (a,b) TEM photo of unmodified SiOH particles. (c) Zeta-potential of sulfonate-modified (SiSO3), unmodified (SiOH), amino-modified (SiNH2) and thiol-modified (SiSH) silica particles at different pHs (10 mMKCl).
126x63mm (150 x 150 DPI)

View Article Online
DOI: 10.1039/C6TB00281A

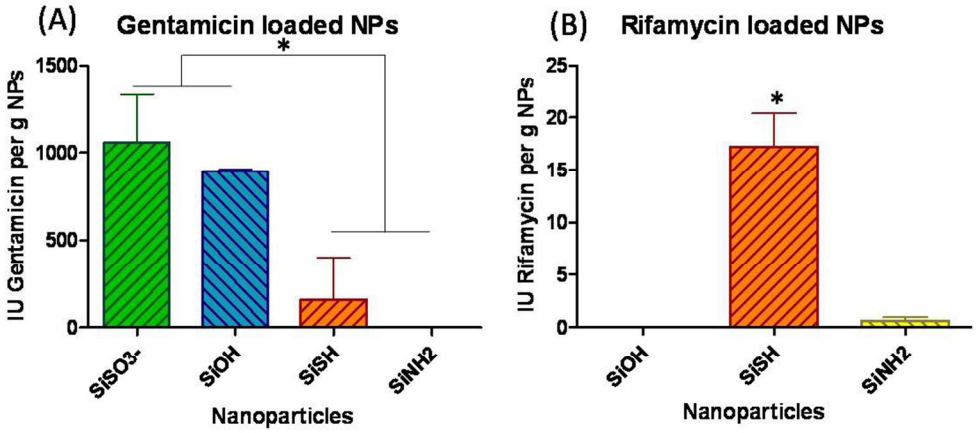

Figure 2: Disk diffusion method evaluation of the antibacterial activity. Activities expressed as International Units (IU) of drug per gram of particles: (A) gentamicin and (B) rifamycin. Results are expressed as mean +/- SD from at least triplicate experiments. * indicates statistical significant difference. ($p < 0.0001$).
192x89mm (150 x 150 DPI)

View Article Online
DOI: 10.1039/C6TB00281A

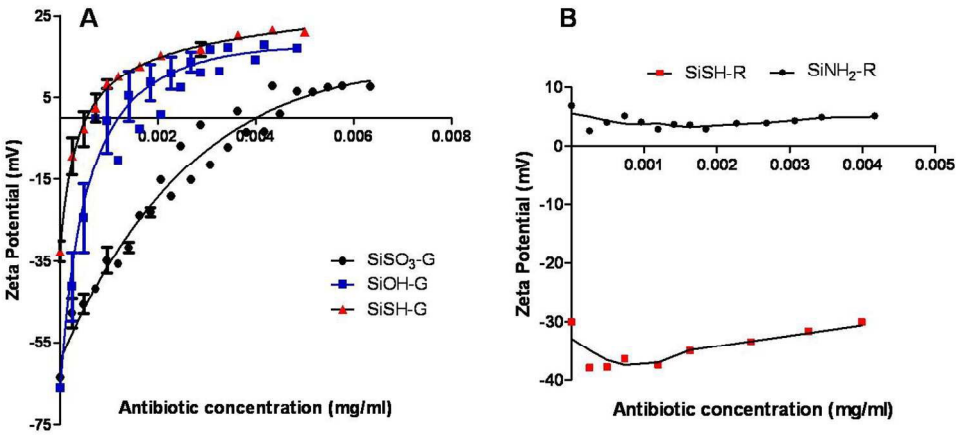

Figure 3: Zeta-potential of silica particles as a function of antibiotic concentration. (A) Gentamicin-loaded sulfonate (SiSO3-G), unmodified (SiOH-G), and thiol (SiSH-G) modified particles. (B) Rifamycin loaded amino (SiNH2-R) and thiol (SiSH-R) modified particles.
247x112mm (150 x 150 DPI)

View Article Online
DOI: 10.1039/C6TB00281A

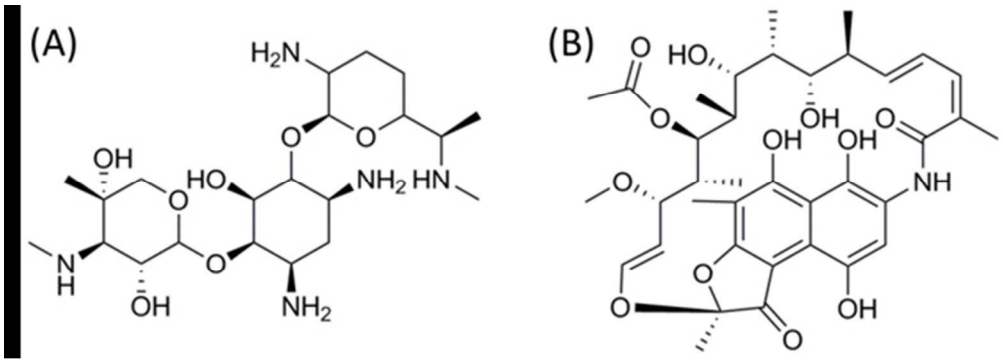

Figure 4: Chemical structures of (A) gentamicin and (B) rifamycin.
108x38mm (150 x 150 DPI)

View Article Online
DOI: 10.1039/C6TB00281A

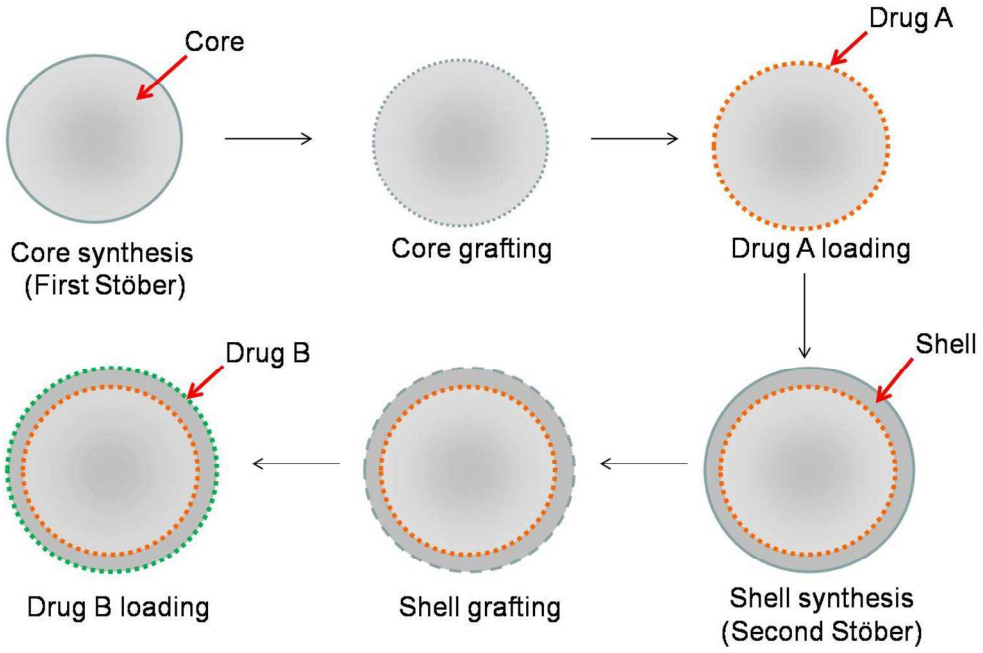

Figure 5: Scheme of the synthesis of double drug-loaded core-shell particles based on a two steps Stöber process.
229x152mm (150 x 150 DPI)

View Article Online
DOI: 10.1039/C6TB00281A

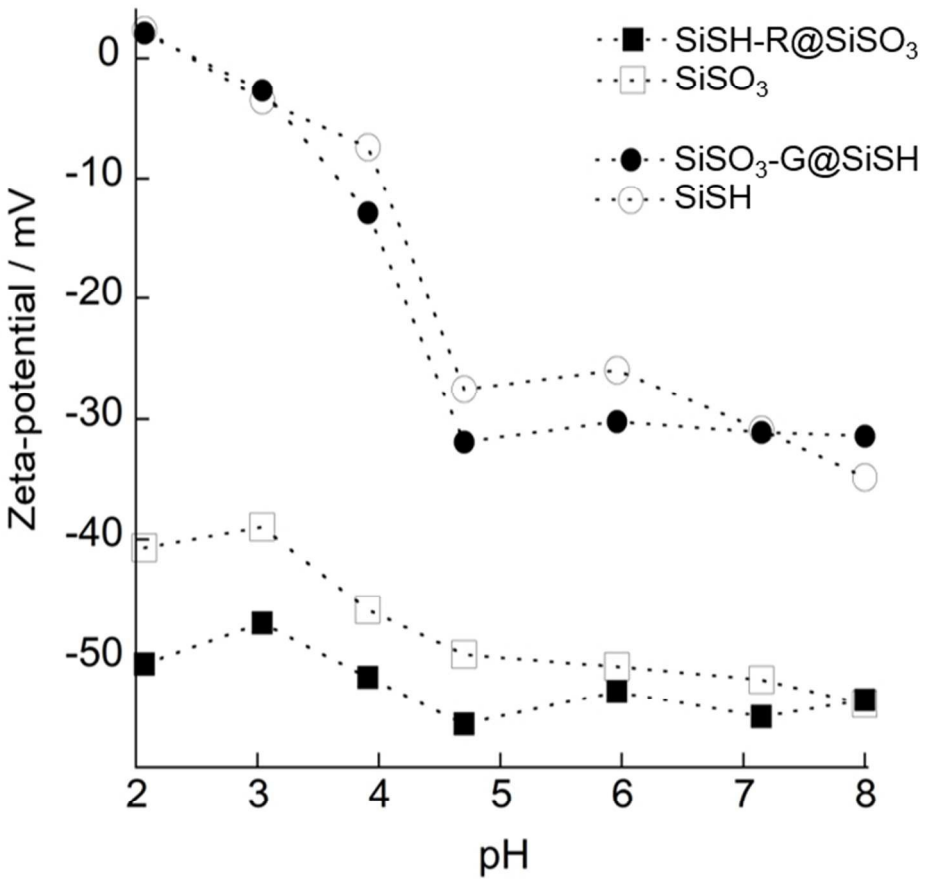

Figure 6: Zeta-potential of silica particles and core-shell particles as a function of pH: SiSH-R@SiSO3 as compared with SiSO3, and SiSO3-G@SH as compared with SiSH.
122x112mm (150 x 150 DPI)

View Article Online
DOI: 10.1039/C6TB00281A

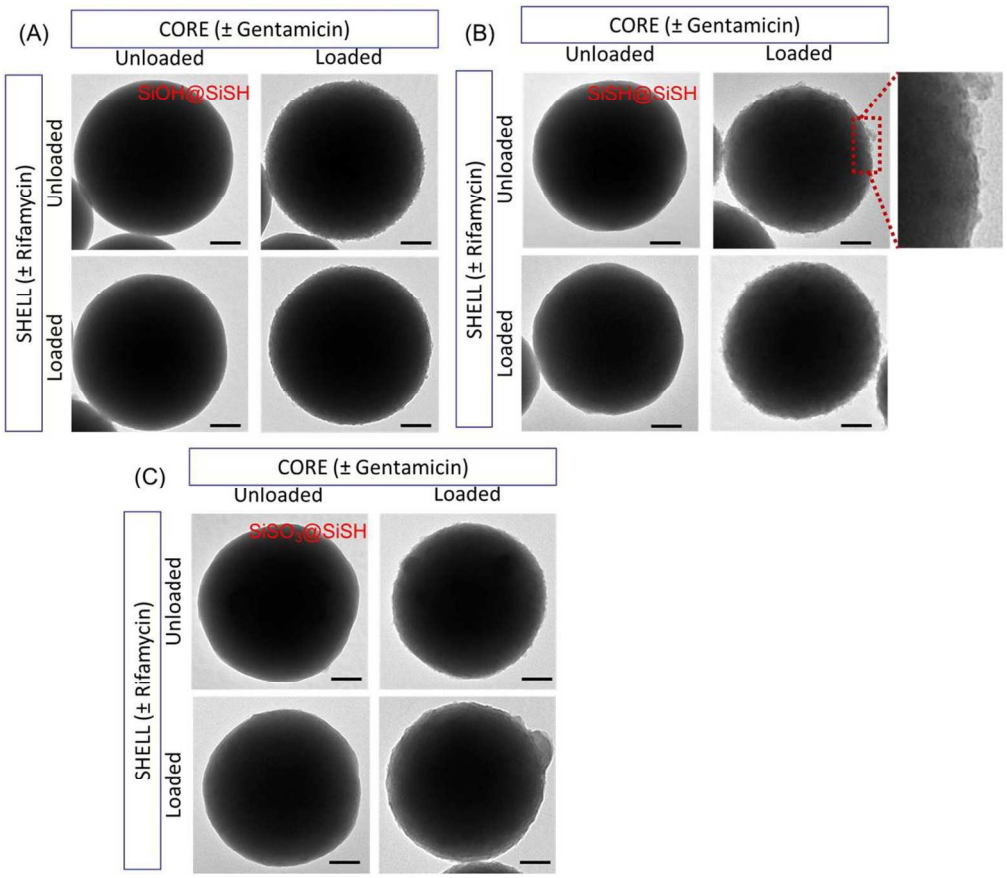

Figure 7: TEM images of: (A) SiOH@SiSH, (B) SiSH@SiSH and (C) SiSO3@SiSHcore-shell particles, with or without gentamicin (G)-loaded core and with or without rifamycin (R)-loaded shell (scale bar 50 nm).
218x190mm (150 x 150 DPI)

View Article Online
DOI: 10.1039/C6TB00281A

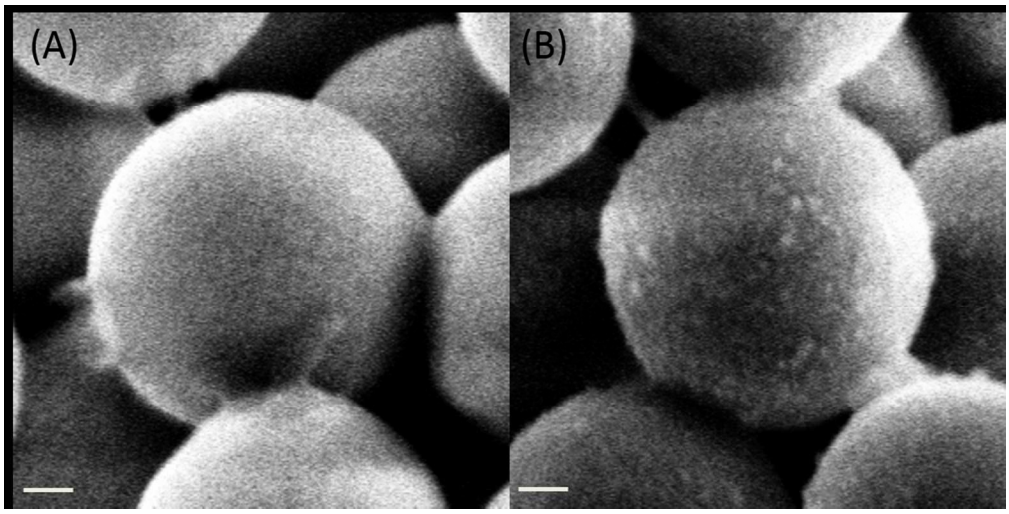

Figure 8: SEM images of (A) SiSO3@SiSH and (B) SiSO3-G@SiSH-R particles (scale bar 50 nm).
201x101mm (150 x 150 DPI)

View Article Online
DOI: 10.1039/C6TB00281A

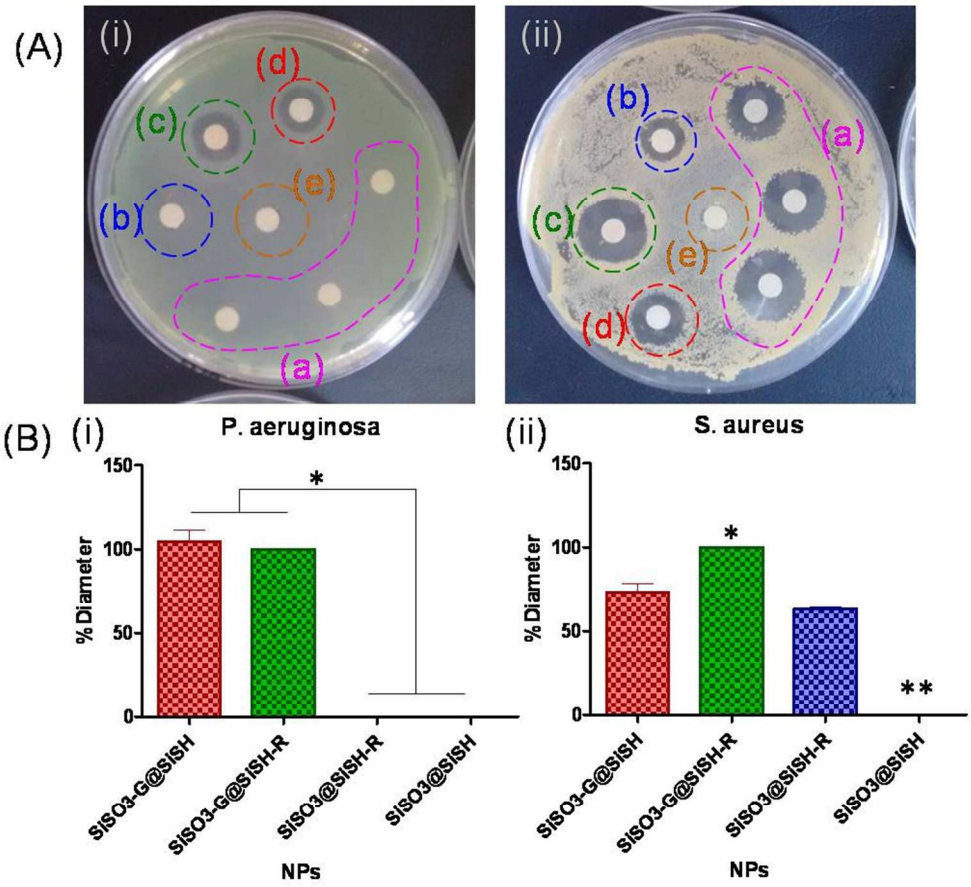

Figure 9: Disk diffusion method evaluation of the antibacterial activity of core-shell particles: (A) plates obtained with (a) rifamycin calibration curve (0.3 – 0.6 – 1.2 µg.ml-1), (b) SiSO3@SiSH-R, (c) SiSO3-G@SiSH-R, (d) SiSO3-G@SiSH and (e) SiSO3@SiSH on (i) P. aeruginosa (ii) S. aureus. (B) Corresponding diameter size relative to SiSO3-G@SiSH-R (100%) for (i) P. aeruginosaand (ii) S. aureus. * and ** indicates statistical significant difference. ($p < 0.0001$).
175x159mm (150 x 150 DPI)

View Article Online
DOI: 10.1039/C6TB00281A

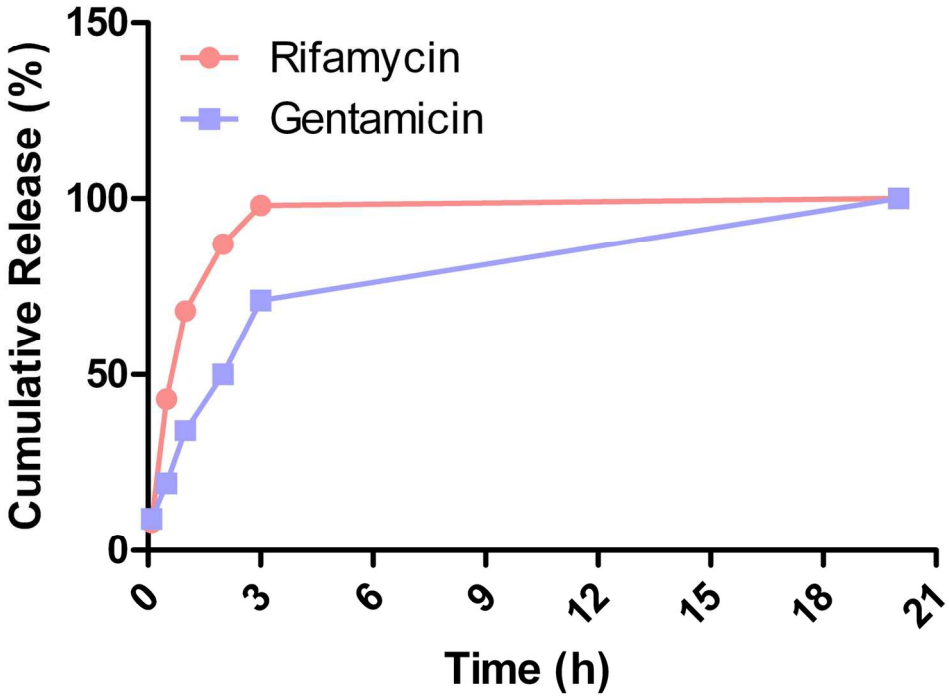

Figure 10: Dual release profiles of rifamicyn and gentamicin from the core-shell particles measured by mass spectrometry.
75x58mm (600 x 600 DPI)

View Article Online
DOI: 10.1039/C6TB00281A

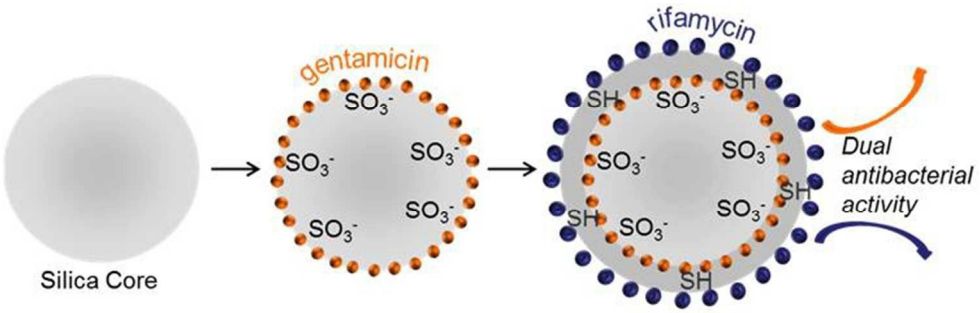

130x40mm (150 x 150 DPI)